Journal of Solid State Chemistry **155,** 427–432 (2000)
doi:10.1006/jssc.2000.8945, available online at http://www.idealibrary.com on IDEAL®

Crystal Structure of Ferroelastic $Pb_5Al_{2.96}Cr_{0.04}F_{19}$ at 300 K

Georges Bravic, Régnault von der Mühll,[1] and Jean Ravez

Institut de Chimie de la Matière Condensée de Bordeaux, Château Brivazac, 87, Avenue du Docteur Albert Schweitzer, 33608 Pessac, France

Received June 15, 2000; in revised form August 3, 2000; accepted August 17, 2000; published online November 29, 2000

Five different phases of $Pb_5Al_3F_{19}$ ([I] to [V]) occur on cooling. The ferroelastic one [III] was stabilized at room temperature by a low rate of Cr–Al substitution. The structure was determined by X-ray diffraction analysis on a single-domain crystal. The symmetry is triclinic, $P\bar{1}$, with cell parameters $a = 10.72(3)$ Å, $b = 10.67(3)$ Å, $c = 7.24(2)$ Å, $\alpha = 109.27(5)^\circ$, $\beta = 110.14(5)^\circ$, $\gamma = 83.33(5)^\circ$. The crystal network, which is closely related to those of the other varieties, is composed of both isolated and trans- corner-linked AlF_6 octahedra developing parallel to the *c*-axis. The structure is closely derived from that of the paraelastic phase [II], mainly by the inclination of the previous tetragonal *c*-axis on the *a*–*b* plane. The loss of the mirror symmetry of the high-temperature phase leads to a break in the Pb^{2+} ion alignment along the 4-fold axis. Polydomain crystals were observed under a polarizing microscope; the ferroelastic [III]–paraelastic [II] phase transition occurs at 326 K on heating.

Key Words: **crystal structure; ferroelastic; triclinic; phase transition; domains; fluoride; lead; aluminum.**

INTRODUCTION

The $Pb_5M_3F_{19}$ (M = Ti, V, Cr, Fe, Ga) compounds undergo a ferroelectric–paraelectric phase transition (1). The interaction between the $6(sp)^2$ lone electron pairs of Pb^{2+} and the volume effects related to the small size of the Al^{3+} cation lead to three additional stable structural modifications (phases II, III, and IV) between the ferroelectric phase V and the paraelectric phase I in $Pb_5Al_3F_{19}$:

$$\underset{I4cm}{V} \underset{120\,K}{\overset{270\,K}{\rightleftarrows}} \underset{P4/n}{IV} \underset{305\,K}{\overset{320\,K}{\rightleftarrows}} \underset{?}{III} \underset{360\,K}{\overset{360\,K}{\rightleftarrows}} \underset{I4/m}{II} \underset{670\,K}{\overset{670\,K}{\rightleftarrows}} \underset{I4/mcm}{I}\ .$$

Phase V is ferroelectric, phase IV antiferroelectric, phase III ferroelastic, phase II paraelastic, and phase I is the paraelectric prototype. Crystal structures of phases II, IV, and V have been previously reported (2–5), and are closely related to each other.

The present work describes the determination of the ferroelastic structure of phase III. There are two challenges in the case of $Pb_5Al_3F_{19}$: first, the crystals are always polydomain and second, phase III is not stable at room temperature but only between 320 and 360 K on heating. Both IV–III and III–II phase transitions correspond to a change of the crystalline system from tetragonal (phases II and IV) to what was previously assumed as monoclinic in phase III (3). Previous preliminary X-ray powder diffraction spectra showed splitting of characteristic lines, implying the disappearance of the 4-fold axis. This ruled out a tetragonal symmetry (6).

A study of the $Pb_5(Al_{1-x}Cr_x)_3F_{19}$ system has recently shown the III–II phase transition temperature to decrease with a rising rate x of Cr–Al substitution (7, 8). The phase diagram in Fig. 1 shows that for compositions $0.87 \leq x \leq 0.95$, phase III becomes stable at 300 K. Since it is possible to determine the structure at room temperature, crystals of composition close to $Pb_5Al_3F_{19}$ but containing a small amount of Cr substituted for Al ($x \approx 0.95$) could be of interest for investigation by X-ray diffraction. Changing the composition but not the structure might also reveal a single-domain ferroelastic crystal.

CRYSTAL GROWTH AND CHEMICAL ANALYSIS

The crystals were grown using the Bridgman method (9). A mixture of PbF_2 and ($0.95AlF_3 + 0.05CrF_3$) was used as starting material. As $Pb_5Al_3F_{19}$ melts incongruently, a small excess of PbF_2 was added to the starting composition, leading to a global ratio $Pb/(Al + Cr) = 6/3$, instead of the stoichiometric value 5/3. The fluoride powders were carefully dried and mixed in a dry glove box. The mixture was then put in a sealed platinum crucible and set in a vertical furnace with a thermal gradient. The temperature of the crucible was maintained for several hours close to 800°C to melt the mixture. The crucible was then withdrawn at a speed close to 1.3 mm/h corresponding to a cooling rate of about 12 deg/hour. A small part of the crystals obtained was milled and analyzed by X-ray diffraction. The powder

[1] To whom correspondence should be addressed. Fax: 33 5 56 84 27 61. E-mail: rvdm@icmcb.u-bordeaux.fr.

0022-4596/00 $35.00

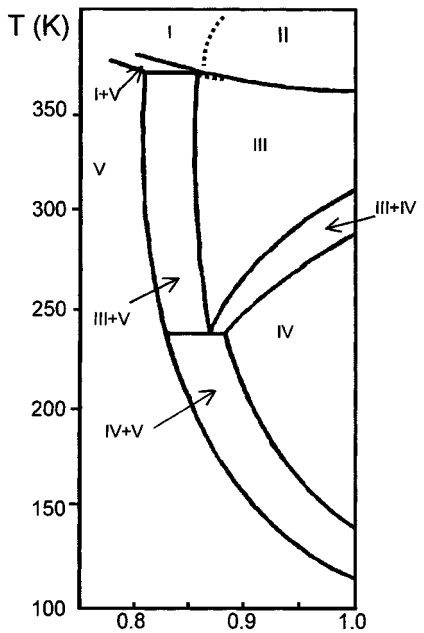

FIG. 1. Phase diagram of the $Pb_5(Cr_{1-x}Al_x)_3F_{19}$ solid solution system as determined on cooling by DTA (7).

spectrum was similar to that of $Pb_5Al_3F_{19}$ (phase III). The chemical composition of some crystals was investigated by electron microprobe analysis. The crystals were included in a polymer wax and then polished. Analysis was done with a Cameca SX1100 system at the CUMEMSE laboratory at the Bordeaux I University. In view of a formulation $Pb_5M_3F_{19}$, the results are consistent with the crystal composition $Pb_5Al_{2.96}Cr_{0.04}F_{19}$ as shown in the following table:

Atom	Atom % (obs)	Atom % (theor) in $Pb_5Al_{2.96}Cr_{0.04}F_{19}$
Pb	18.96(21)	18.518
Al	10.98(08)	10.963
Cr	0.14(04)	0.148
F (by difference from 100)	69.91	70.371

CRYSTAL STRUCTURE DETERMINATION

Experimental

Most of the as-grown crystals showed ferroelastic domains. However, with the aid of a polarizing microscope, an exceptionally domain-free crystal was selected to be used for structure determination. This single-domain crystal ($0.05 \times 0.05 \times 0.015$ mm) was mounted on an Enraf-Nonius CAD4 diffractometer and analyzed using monochromatic Mo$K\alpha$ X-ray radiation ($\lambda = 0.7069$ Å). Unit cell parameters were obtained by least-squares refinement from 25 centered reflections in the range $11.3° \leq \theta \leq 22.3°$. The intensities of three standard reflections each monitored for 2 hours revealed no significant decay during data collection.

The determination of the symmetry was mainly based on the examination of the reflected intensities. A reliability factor based on the values of the measured intensities and their equivalents by symmetry operators $R(\text{int.}) = \sum|F - \langle F\rangle|/\sum\langle|F|\rangle$ is reported in the following table assuming all possible locations of the 2-fold axis in the tetragonal reciprocal cell:

TABLE 1
Crystal Data for the Paraelastic (II), Ferroelastic (III), and Antiferroelectric (IV) Phases of $Pb_5Al_3F_{19}$ Type

Formula	$Pb_5Al_3F_{19}$	$Pb_5Al_{2.96}Cr_{0.04}F_{19}$	$Pb_5Al_3F_{19}$
Phase	II	III	IV
Temperature (K)	370	298	298
M (g.mol^{-1})	936.2	937.2	936.2
Crystal system	Tetragonal	Triclinic	Tetragonal
Space group	$I4/m$	$P\bar{1}$ [$I\bar{1}$]	$P4_1/n$
a (Å)	14.285(7)	10.72(3) [14.26(5)]	20.13(2) [14.23(1)]
b (Å)	$= a$	10.67(3) [14.22 (4)]	$= a$
c (Å)	7.227(3)	7.24(2)	7.220(1)
α (°)	90	109.27(5) [89.30(6)]	90
β (°)	90	110.14(5) [89.89(3)]	90
γ (°)	90	83.33(5) [89.99(8)]	90
V (Å^3)	1475(1)	734(9) [1468(18)]	2939(1) [1470(1)]
Z	4	2	8
D_{calc} (g.cm^{-3})	6.66	6.69	6.68
λ (Mo$K\alpha$), (Å)	0.71069	0.71069	0.71069
μ (mm^{-1})	56.6	56.6	56.6
θ range (°)	10 to 26	2 to 25	2 to 30
hkl ranges	h: -20 to 20	h: -12 to 12	h: -28 to 28
	k: -20 to 20	k: -12 to 12	k: -28 to 28
	l: 0 to 10	l: 0 to 8	l: 0 to 10
Collected reflections	5787	2793	18502
Unique reflections	1715	2583	3527
R(int)	0.065	0.026	0.048
		Structure Refinement	
Refinement based on	F	F^2	F^2
Reflections used	1115	2522	1276
Number of parameters	52	224	138
R^a	0.053	0.065	0.058
wR^a	0.058	0.201	0.065
S (goodness of fit)	1.12	1.11	1.84
Δ/σ (max)	0.1	0.1	0.3
Residual density (e.Å^{-3})	5	6	6

[a] $R = \sum||F_o| - |F_c||/\sum|F_o|$ for observed reflections. $wR = [\sum w(F_o^2 - F_c^2)/\sum wF_o^2]^{1/2}$, $w = 1/(\sigma^2(F^2) + 0.04F_o^2)$.

Symmetry element	R(int.) (%)	Resulting symmetry
2-fold axis along c^*	12.21	
2-fold axis along b^*	15.62	
2-fold axis along a^*	16.43	Monoclinic
2-fold axis along [[1 1 0]]	16.26	
2-fold axis along [[1 −1 0]]	16.80	
Inversion center only, −1	2.51	Triclinic

This table makes it possible to select the triclinic symmetry. Thus, the structure was solved by least-squares refinement starting from the triclinic transformed phase II locations of the ions. Structure refinement based on F^2 was carried out by the full-matrix method. Scattering factors were taken from *International Tables for Crystallography* (11). The Pb^{2+} ions were refined with anisotropic thermal parameters and the other ions with isotropic thermal parameters. Final reliability factors converged to $R(F) = 0.065$ and $wR(F^2) = 0.201$. Crystal data and details of data collection and refinement are given in Table 1. For easier comparison, the previous results for the phases II and IV are also given. The phase III and IV parameters are also described as compared to the phase II ones and are enclosed between brackets. A final difference Fourier map showed a residual density of 6 e.$Å^{-3}$ near the Pb positions. This effect should be considered as a consequence of the limitation of the Ewald's sphere used for data collection. The final positional parameters are listed in Table 2. Calculations were carried out using programs written or modified locally and illustrations in the CrystalMaker (12) software.

TABLE 2
Fractional Atomic Coordinates and Equivalent or Isotropic Thermal Parameters (Å²)

	x	y	z	B_{eq}/B_{iso}[a]
Pb(11)	0.3245(1)	−0.1546(2)	0.0782(2)	1.97(4)
Pb(12)	0.1542(2)	0.3247(2)	0.2332(2)	1.93(4)
Pb(21)	−0.1570(1)	0.2792(1)	0.5614(2)	1.58(4)
Pb(22)	0.2778(1)	0.1549(2)	0.7153(2)	1.63(4)
Pb(3)	−0.4833(2)	0.5305(3)	0.2753(3)	4.02(7)
Al(11)	−0.1684(7)	0.4846(7)	0.159(1)	1.08(5)
Al(12)	−0.4843(7)	−0.1685(7)	−0.321(1)	0.94(5)
Al(2)	0.0035(7)	0.0014(7)	0.249(1)	0.91(5)
F(1)	0.0000	0.0000	0.0000	3.3(2)
F(2)	0.0000	0.0000	0.5000	1.3(1)
F(31)	−0.065(2)	0.834(2)	0.632(2)	1.7(1)
F(32)	0.061(2)	−0.836(2)	−0.145(2)	2.0(1)
F(33)	−0.839(2)	−0.062(2)	−0.204(2)	1.9(1)
F(34)	0.833(2)	0.066(2)	0.695(3)	2.2(1)
F(41)	−0.218(2)	0.604(2)	0.373(2)	1.8(1)
F(42)	0.201(2)	−0.612(2)	−0.035(3)	2.2(1)
F(43)	−0.614(1)	−0.194(1)	−0.237(2)	1.3(1)
F(44)	0.603(2)	0.219(2)	0.579(2)	1.7(1)
F(51)	0.139(2)	0.642(2)	1.068(3)	2.7(1)
F(52)	−0.155(2)	−0.650(2)	0.264(2)	2.0(1)
F(53)	−0.645(2)	0.160(2)	0.419(2)	1.9(1)
F(54)	0.639(2)	−0.123(2)	0.944(3)	2.4(1)
F(61)	0.004(2)	0.523(2)	0.276(3)	2.4(1)
F(62)	−0.523(2)	0.006(2)	−0.284(2)	2.1(1)
F(71)	0.344(2)	0.560(2)	0.960(3)	2.2(1)
F(72)	−0.561(2)	0.343(2)	0.351(3)	2.5(1)
F(81)	0.290(2)	0.538(2)	0.411(2)	1.7(1)
F(82)	−0.539(1)	0.287(1)	−0.128(2)	1.5(1)

Anisotropic Thermal Motion (Å²)

	U_{11}	U_{22}	U_{33}	U_{12}	U_{13}	U_{23}
Pb(11)	0.0194(7)	0.0432(9)	0.0269(8)	0.0044(6)	0.0083(6)	0.0149(6)
Pb(12)	0.0302(8)	0.0318(8)	0.0260(7)	−0.0030(6)	0.0100(6)	0.0111(6)
Pb(21)	0.0202(7)	0.0277(8)	0.0238(7)	0.0050(5)	0.0081(5)	0.0111(6)
Pb(22)	0.0142(7)	0.0356(8)	0.0237(7)	−0.0033(5)	0.0036(5)	0.0126(6)
Pb(3)	0.052(1)	0.087(2)	0.049(1)	0.008(1)	0.0175(9)	0.038(1)

[a] $B_{eq} = (8\pi^2/3)\sum_i \sum_j U_{ij}\, a_i^*\, a_j^*\, a_i\, a_j$.

Structure Description

The structural packing of the different of $Pb_5Al_3F_{19}$ phases can be described as an octahedral AlF_6 arrangement and lead distribution in unit cell (Figs. 2 and 3).

There are two types of fluoaluminate octahedra:

(1) The free ones are located near the 0 and 1/2 levels of the c parameter of the reference cell (tetragonal, phase II). A unique kind of AlF_6 related to Al(1) is present in the phase II structure; it is located on the mirror of the crystal cell. This mirror disappears in phase III as in phase IV, thus allowing a slight inclination away from the previous special position ($\sim 3^\circ$ for phase III and 9° for phase IV). The loss of

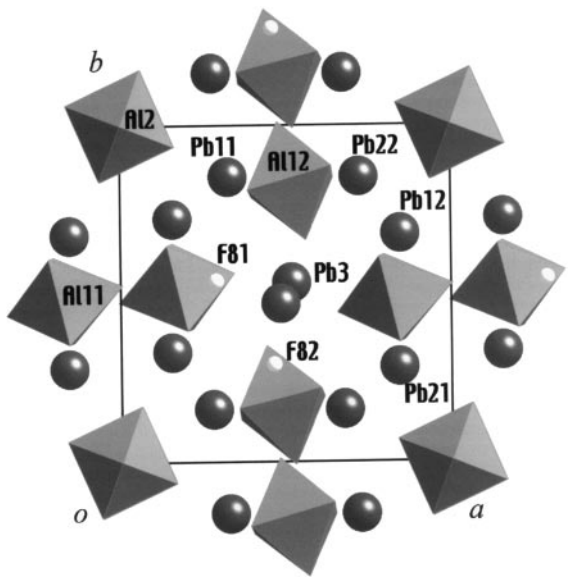

FIG. 2. Projection of the structure of $Pb_5Al_{2.96}Cr_{0.04}F_{19}$ along c.

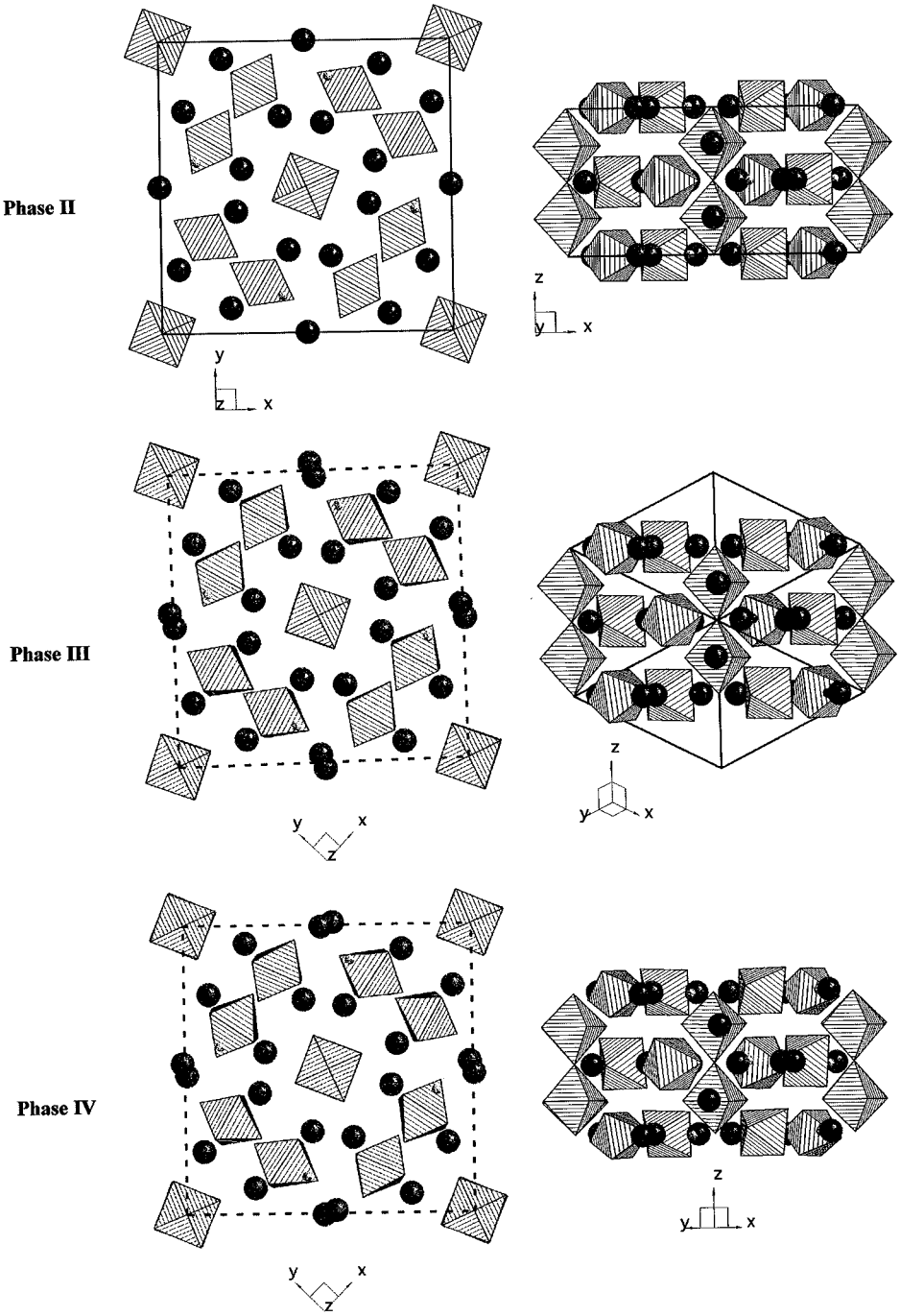

FIG. 3. Comparison of the paraelastic (II), ferroelastic (III), and antiferroelectric (IV) phases of $Pb_5Al_3F_{19}$.

the 4-fold axis in phase III allows the presence of two independent free octahedra related to Al(11) and Al(12). The same result is obtained in phase IV by cell doubling.

(2) The corner-linked octahedra form a chain along the *c* direction. The shared fluorine atoms F(1) and F(2) are located on inversion centers. The maximum shifts of Al^{3+} cations in the *c* direction from the centers of their octahedron are in the range of experimental errors for phase II, 0.03(2) Å, and phase III, 0.02(1) Å. For phase IV, alternate and significant displacements, 0.08(2) Å, indicate its antiferroelectric properties. All of these linked octahedra overlap in projection along the *c* direction, except for the Al(23) chain of phase IV which shows a twist of 2.7° between two adjacent octahedra.

Moreover, there are two types of Pb^{2+} arrangements:

(1) Pb(1x) and Pb(2x) are on (phase II) or near (phase III and IV) the zero and 1/2 levels of the *c* parameter of the tetragonal cell. They are irregularly surrounded by eight F^- anions (see Table 3). It should be noticed that there is a short distance Pb(2x)–F(8x), 2.27 ± 0.1 Å; F(8x) corresponds to a lone fluorine outside of the AlF_6 octahedra.

(2) In phase III, the Pb(3) cations are aligned in the *c* direction at the 1/4 or 3/4 level. In the other phases, this alignment is broken and three consecutive Pb(3) cations form angles of 157.8° in phase III and 160.0° in phase IV. All of the planes containing the Pb(3) chains are parallel in phase III; in phase IV, the chains are shared in two orthogonal directions. This is the main difference between the phase III and phase IV crystal structures.[2]

DOMAIN WALL PATTERN AND PHASE TRANSITIONS OF THE CRYSTALS

In a phase transition like II → III corresponding to a symmetry change $4/mF\bar{1}$, the only possible domain walls correspond to two families of planes parallel to the *b* axis and perpendicular to each other (9). A crystal plate with the larger face oriented parallel to the (010) plane was observed at room temperature with transmitted polarized light. Two kinds of ferroelastic perpendicular domain walls can be seen in Fig. 4. The optical axis was oriented along *c*, parallel to the future 4-fold axis to appear in phase II. The phase transitions can be observed under the polarizing microscope by varying the temperature of the crystal plate, using a nitrogen temperature-controlled gas stream. After a previous cooling, the crystal was slowly heated and ferroelastic domains appeared close to 300 K and disappeared again at 326 K. Successive heating and cooling cycles revealed the following phase transition sequence:

$$\text{IV} \; -300\,\text{K} \; \rightarrow \; \text{III} \; -326\,\text{K} \; \rightarrow \; \text{II} \quad \text{on heating;}$$

$$\text{II} \; -325\,\text{K} \; \rightarrow \; \text{III} \; -276\,\text{K} \; \rightarrow \; \text{IV} \quad \text{on cooling.}$$

These observations on a relatively large crystal (1 mm) do not exactly fit with the phase diagram given in Fig. 1 for which fine grained powder (5 μm) was used. In view of the pseudo-monoclinic cell derived from that of the phase II with $\alpha = 89.30$ (see Table 1), an approximation of the spontaneous deformation $\delta_s = 1/(2\cos\alpha) = 61 \times 10^{-4}$ can be given. This relatively low value leads us to expect ferroelastic properties for this material.

[2] Labeling conventions: All of the elements are labeled in reference to the high-symmetry phase II structures. When an element [ex.: Al(2)] splits into various new elements by loss of symmetry, the new numbers result from the concatenation of the old number and the order of the new elements [ex.: Al(21) and Al(22)]. Any member of this family will be designated by the order $\times$[ex.:Al(2$\times$)].

TABLE 3
Bond Lengths (Å)

	Phase II	Phase III		Phase IV	
		Isolated AlF_6 Octahedra			
	Al(1)	Al(11)	Al(12)	Al(11)	Al(12)
Al(1)–F(4)	1.82(1)	1.85(2)	1.81(2)	1.73(4)	1.86(4)
		1.78(2)	1.77(2)	1.71(4)	1.92(4)
Al(1)–F(5)	1.78(1)	1.85(2)	1.87(2)	1.72(4)	1.80(4)
		1.80(2)	1.79(2)	1.75(4)	1.86(4)
Al(1)–F(6)	1.75(2)	1.78(3)	1.82(2)	1.78(4)	1.84(4)
Al(1)–F(7)	1.81(2)	1.84(2)	1.84(2)	1.79(4)	1.80(4)
		Top-Linked AlF_6 Octahedra			
	Al(2)	Al(2)		Al(21)	Al(22) Al(23)
Al(2)–F(1)	1.778(5)	1.785(9)		1.72(2)	1.73(3) 1.76(1)
Al(2)–F(2)	1.836(5)	1.835(9)		1.88(2)	1.88(3) 1.85(1)
Al(2)–F(3)	1.787(9)	1.77(2)		1.78(4)	1.77(5) 1.81(4)
		1.79(2)			1.79(4)
		1.76(2)			
		1.78(2)			
		Neighboring of *c*-Aligned Pb(3) Ions			
Pb(3)–F(7)	2.50 (1)	2.53(2)		2.50(4)	
	[×4]	2.48(2)		2.48(4)	
		2.53(2)			
		2.49(2)			
Pb(3)–F(8)	2.80(1)	2.90(2)		2.73(4)	
	[×4]	2.74(2)		2.71(4)	
		2.58(2)		2.61(8)	
Pb(3)–F(4)		2.82(2)		2.79(4)	
		2.86(2)		2.92(4)	
Pb(3)–F(6)				2.55(4)	
				2.59(4)	
		Neighboring of the Pb(1) and Pb(2) Ions			
	Pb(1)	Pb(11)	Pb(12)	Pb(11)	Pb(12)
Pb(1)–F(3)	2.609(9)	2.59(2)	2.62(2)	2.46(4)	2.69(4)
	[×2]	2.64(2)	2.62(2)	2.62(4)	2.68(4)
Pb(1)–F(4)	2.517(9)	2.48(2)	2.55(2)	2.51(4)	2.71(4)
	[×2]	2.63(2)	2.47(2)	2.36(4)	2.57(4)
Pb(1)–F(5)		2.86(2)	2.87(2)	2.95(4)	2.85(4)
				2.96(4)	
Pb(1)–F(6)	2.54(1)	2.51(2)	2.51(2)	2.50(4)	2.81(4)
	[×2]				
Pb(1)–F(7)	2.83(1)	2.88(2)	2.88(2)	2.88(4)	2.54(4)
	[×2]				
Pb(1)–F(8)	2.60(1)	2.54(2)	2.55(2)	2.64(4)	2.54(8)
	[×2]				
	Pb(2)	Pb(21)	Pb(22)	Pb(21)	Pb(22)
Pb(2)–F(3)	2.802(9)	2.84(2)	2.78(2)	2.88(4)	2.68(4)
	[×2]	2.77(2)	2.82(2)	2.85(4)	2.73(4)
Pb(2)–F(4)	2.785(9)	2.74(2)	2.80(2)	2.83(4)	2.74(4)
	[×2]	2.78(2)	2.78(2)	2.84(4)	2.69(4)
Pb(2)–F(5)	2.521(9)	2.48(2)	2.57(2)	2.59(4)	2.42(4)
	[×2]	2.51(2)	2.44(2)	2.61(4)	2.49(4)
Pb(2)–F(6)	2.53(1)	2.52(2)	2.51(2)	2.54(4)	2.54(4)
	[×2]				
Pb(2)–F(8)	2.27(1)	2.27(2)	2.28(2)	2.29(4)	2.24(4)
	[×2]				

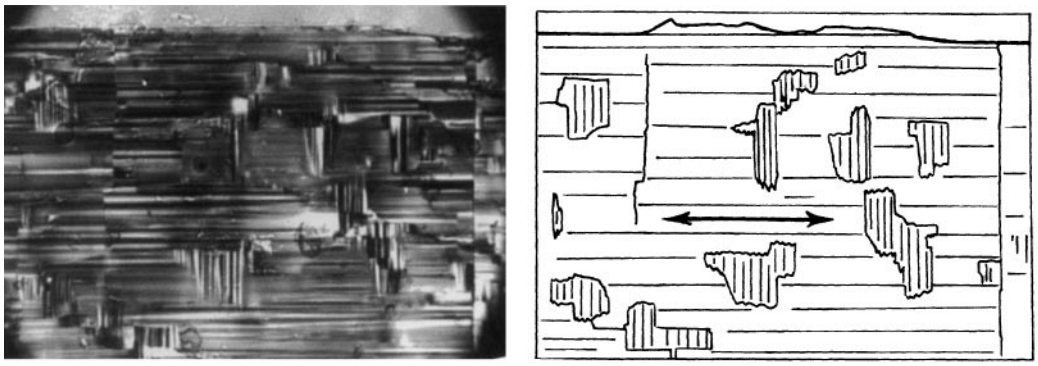

FIG. 4. Domain wall pattern in a (010) $Pb_5Al_{2.96}Cr_{0.04}F_{19}$ crystal plate.

CONCLUSION

The $Pb_5Al_3F_{19}$ compound has five different phases. A low rate of Cr–Al substitution has allowed us to obtain a single–domain crystal whose ferroelastic phase [III] remains stable at room temperature. X-ray diffraction measurements show the symmetry to be triclinic.

The structure derives closely from that of the tetragonal paraelastic phase [II], mainly by the inclination of the previous tetragonal *c*-axis on the *a*–*b* plane. In the triclinic phase, the loss of the mirror symmetry of the high-temperature phase [II] leads to a break in the Pb^{2+} ion alignment along the 4-fold axis. This involves displacements which occur in planes which are all parallel in the ferroelastic phase and are shared between two families with perpendicular directions in the antiferroelectric phase [IV]. The loss of the mirror symmetry allows also slight rotations of the AlF_6 isolated octahedra.

ACKNOWLEDGMENTS

The authors thank J.-P. Chaminade for crystal synthesis.

REFERENCES

1. J. Ravez and S. C. Abrahams, *C. R. Acad. Sci., IIc* **1,** 15 (1998).
2. V. Andriampianina, P. Gravereau, J. Ravez, and S. C. Abrahams, *Acta Crystallogr. B* **50,** 135 (1994).
3. J. Ihringer, J. Ravez, and S. C. Abrahams, *Z. Krist.* **209,** 853–857 (1994).
4. S. Sarraute, J. Ravez, G. Bravic, D. Chasseau, and S. C. Abrahams, *Acta Crystallogr. C* **51,** 1731 (1995).
5. S. Sarraute, J. Ravez, R. Von der Mühll, G. Bravic, G. Feigelson, and S. C. Abrahams, *Acta Crystallogr. B* **52,** 72 (1996).
6. S. Sarraute, Thèse, Université Bordeaux I, 1995.
7. J. Ravez, V. Andriampianina, A. Simon, L. Rabardel, J. Ihringer, and S. C. Abrahams, *J. Appl. Crystallogr.* **27,** 352 (1994).
8. J.-M. Réau, M. El Omari, and J. Ravez, *Phase Trans.* **69,** 227–236 (1999).
9. J. Sapriel, *Phys. Rev. B* **12,** 5128–5140 (1975).
10. J. P. Chaminade, ICMCB-CNRS, private communication.
11. International Tables for Crystallography, (A. J. C. Wilson and E. Prince, Eds.), Kluwer Academic Publishers. Vol. C, Tables 4.2.6.8 and 6.1.1.4 (1999).
12. D. Palmer, Crystal Maker 4, P.O. Box 183, Bicester, Oxfordshire, OX6 7BS, U.K., 1999.